Archimedes optimization algorithm based extremum seeking control maximum power point tracking for enhancing performance and efficiency of photovoltaic systems

Cite as: AIP Conference Proceedings **2776**, 060004 (2023); https://doi.org/10.1063/5.0137307
Published Online: 12 April 2023

Hamid A. Abed Hannon, Ahmad T. Abdulsadda and Haider K. Latif

Archimedes Optimization Algorithm Based Extremum Seeking Control Maximum Power Point Tracking for Enhancing Performance and Efficiency of Photovoltaic Systems

Hamid A. Abed Hannon[1,a)], Ahmad T. Abdulsadda[2, b)],and Haider K. Latif [1,c)]

[1]*Al-Furat Al-Awsat Technical University, Technical College of Al-Mussaib, Babylon, Iraq*
[2]*Al-Furat Al-Awsat Technical University, Al Najaf Technical Engineering College, Najaf, Iraq*

[a)] Corresponding author: hamidali.tcm.24@student.atu.edu.iq
[b)]coj.abdulsad@atu.edu.iq
[c)]dr-haider.k.latif@atu.edu.iq

Abstract. Slow reaction owing to fixed-step change, high ripple, and increased oscillation due to swings around maximum power point are the main drawbacks of conventional Maximum Power Point Tracking (MPPT). This study proposes a hybrid MPPT control to address these concerns .In this study we used the Extremum Seeking Control(ESC) based on a metaheuristic Archimedes Optimization Algorithm (AOA) to achieve MPPT in PV panels under non-uniform conditions. Two parameters of the extremum-seeking control is tuned using the Archimedes optimization algorithm. The proposed system parameters is examined by simulation using MATLAB/Simulink. According to the simulation results, the proposed MPPT effectively achieves the MPP under any non-uniform situation with less overshoot, oscillation and ripple compared to traditional MPPT. The suggested MPPT has an efficiency of up to 99.65%.

***Keywords*.** hybrid MPPT; AOA-ESC MPPT; Archimedes optimization algorithm; Luo DC-DC converter; PV system.

INTRODUCTION

We can't survive without energy, and it's critical to economies and societies progress [1,2]. Coal, gas, and oil are responsible for roughly 87% of the world's total energy production, whereas nuclear power plants are responsible for only 6%. Solar, geothermal, wind, hydropower, and biofuels account for the remaining 7% of global energy use [3,4]. Solar energy's quantity, renewability, and cleanliness energy have prompted numerous investigations in the last two decades. A photovoltaic (PV) panel converts solar irradiance into electrical energy straight from the sun [5,6]. Some downsides to solar PV panels include low efficiency (less than 22.5 percent), production costs for energy, and reliance on environmental factors [5,7-9]. A PV cell's current and voltage characteristics curve are non-linear under varying solar irradiances, temperatures, and loads [10,11]. The P-V curve produces only one maximum power point (MPP) when using conventional maximum power point tracking (MPPT) algorithms [12,13]. Creative methods had to be found to overcome these drawbacks. There are a variety of ways to maximize the output of a PV panel's maximum power point. The characteristic current–voltage and power–voltage curves show many peaks under Partial Shading Conditions (PSCs), making it difficult to follow true MPP with MPPT control technologies [14].

PV cell power trackers commonly employ the Perturb and Observe (PO) method. A PV array has some disadvantages even though it can track its maximum power point with the PO technique, including the requirement that ambient conditions be constant or fluctuate slowly. When using the PO method, losses can be avoided by using the Incremental Conductance (IC) technique [15]. A photovoltaic system's current-to-voltage ratio (dI/dV) is

1st International Conference on Achieving the Sustainable Development Goals
AIP Conf. Proc. 2776, 060004-1–060004-15; https://doi.org/10.1063/5.0137307
Published by AIP Publishing. 978-0-7354-4441-6/$30.00

equivalent to the increased conductance (dI/dV) when using the integrated circuit (IC) approach. As a result of the duty cycle step size modification, this method provides high tracking speed but also generates additional oscillations and poor dynamics, making it unsuitable for detecting MPP in steady-state and transient stages [16].
Control is a key component of the approaches described here. Extremum Seeking Control (ESC) is a term used in the field of control systems to describe a variety of methods for determining the best point of system performance. Searching for extreme points in random features is made easier by the ESC method, an adaptive closed-loop control technique. When the MPPT system kicks in, the output power of the PV cells begins to ripple and then drops. This is due to the ESC's dithering signal frequency. Under conditions of partial shading, there is also an interference of the local maximum power point (MPP) [17].
In this study, a hybrid optimization technique for tracking maximum power point in solar cells that is based on ESC method is evaluated and compared to perturb and observe (PO), incremental conductance (IC) and classic ESC approaches. The proposed system is proved by simulation using MATLAB/Simulink. The simulation results obtained by the proposed MPPT have achieved the MPP under non-uniform conditions with less overshoot, oscillation and ripple compared to other trackers, hence the performance and efficiency of PV system is improved.

PHOTOVOLTAIC SYSTEM

Figure 1. illustrates the proposed photovoltaic system utilized to generate power by simulations. As shown the system consists of solar panel, a super-lift Luo DC/DC converter, a hybrid MPPT control, and a local load. The maximum power tracker controls the DC/DC converter to get best power of solar energy. The PV system's overall power output is chosen to be 2340 W.

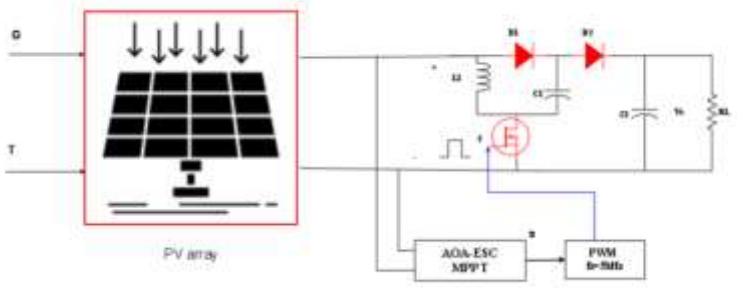

FIGURE 1. Proposed system configuration

MODELING OF SOLAR PANEL

Modelling PV arrays for changed environmental conditions is a energetic subject in designing the size of a PV plant and its MPPT controller [18]. The solar panel equivalent circuit can be modeled as a current source and a diode connected in parallel. Series resistors R_s and parallel resistors R_{sh} are used to represent the conduction losses as shown in Figure 2 [19].

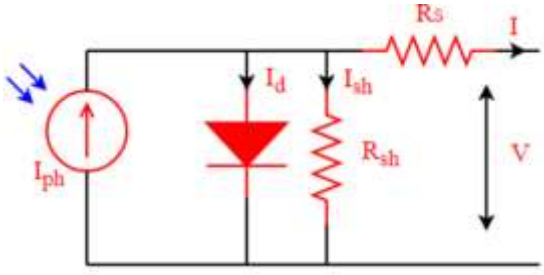

FIGURE 2. Equivalent circuit diagram of the solar panel

Equation (1) can be obtained by applying Kirchhoff's law :

$$I_{PV} = I_{Ph} - I_D - I_{sh} \quad (1)$$

Where I_{Ph} is the photocurrent generated by the photovoltaic cells. I_D is the diode current and I_{sh} is the loss resistor current. I_{Ph} depends on climatic conditions as follows:

$$I_{ph} = [I_{SC} + K(T - T_{STC})]\frac{G}{G_{STC}} \quad (2)$$

Where I_{sh} is the short circuit current, K is the solar cell temperature coefficient, T is the temperature, and G is the irradiance. T_{STC} and G_{STC} are temperature and irradiance under standard Test Conditions (STS). In turn, the diode current I_D can be expressed as follows:

$$I_D = I_O \exp[\frac{q\,(I_{PV}\,Rs + V_{PV})}{(n\,k\,T\,N_S)} - 1] \quad (3)$$

Where I_O is the current of saturation, q is the charge of electron, n is the diode ideality factor, k is the Boltzmann's constant and Ns is the number of cells connected in series. The saturation current I_O is given as follows:

$$I_O = I_{rs}\left(\frac{T}{T_{STC}}\right) \exp[\frac{q\,E_g}{n\,k}(\frac{1}{T_{STC}} - \frac{1}{T}) \quad (4)$$

Where E_g is the semiconductor bandgap energy. I_{rs} is the reverse saturation current and can be expressed as follows:

$$I_{rs} = I_{sc}[\exp\left(\frac{q\,V_{oc}}{n\,k\,T\,N_s} - 1\right)]^{-1} \quad (5)$$

In turn, I_{sh} can be expressed as follows:

$$I_{sh} = \frac{I_{PV}\,Rs + V_{PV}(\frac{V_P}{N_s})}{Rsh} \quad (6)$$

Where N_p is the number of cell connected in parallel. Considering the parallel-connected equation (1) can be rewritten as:

$$I_{PV} = I_{Ph}\,(N_P - I_D)(N_P - I_{sh}) \quad (7)$$

In PV systems, A DC-DC step-up converter is used to regulate and raise the voltage generated by PV modules. Two diodes (D1 and D2), an inductor (L), two capacitors (C1 and C2) and on switch (S) are used to make up the super-lift luo Convertor [20]. L, C_1 and C_2 are given in (8), (9) and (10) respectively.

$$L = \frac{D\,V_{in}}{f_S\,\Delta I_{L1}} \quad (8)$$

$$C_1 = \frac{I_{in}\,(1-D)}{(2-D)\,f_S\,\Delta V_{C1}} \quad (9)$$

$$C_2 = \frac{1-D}{2\,R\,f_S\,\Delta V_{C2}} \quad (10)$$

The elementary circuit of the super-lift luo Convertor is shown in Figure 3. The circuit modeling is giving in equations (11) (on-state), (12) (off-state) and (13) the output voltage gain respectively [21].

$$Vin = VL = Vc1 = L\Delta i/dt \quad (11)$$

$$\Delta i = \frac{VL(1-D)T}{L} = Vo - 2Vin(1-D)T/L \quad (12)$$

$$G = \frac{Vo}{Vin} = \frac{2-D}{1-D} \quad (13)$$

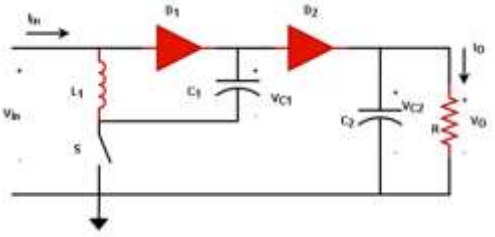

FIGURE 3. Elementary circuit of the super-lift luo convertor

ARCHIMEDES OPTIMIZATION ALGORITHM

The Archimedes optimization algorithm (AOA) [22], which is based on Archimedes' principle, which is regarded as a physical rule. The Archimedes principle is concerned with the object that is either entirely or partially submerged in the fluid. As the liquid on the body generates an upward push (known as buoyancy), this force. is equivalent to the amount of fluid that was expelled from the body. The items submerged in water are referred to as "population individuals" in AOA (candidate solutions). Randomly placing each object in the problem search area is the first step in this method. The fitness function corresponding to that value is then determined. Iteratively, AOA changes object densities and volumes, as well as their accelerations, based on collisions with neighboring objects. The formula used to initialize all objects is as follows...

Initialization

The position initializing of all objects can be expressed as:

$$O_i = lb_i + rand \times (ub_i - lb_i); i = 1.2. \ldots . N \quad (14)$$

Where O_i is the ith item in a population of N. There are ub_i and lb_i at the bottom and top of the search space, respectively.

For the sake of randomness, we can use equation (15), which shows the volume (vol) and density (den) of each ith object:

$$den_i = rand$$

$$vol_i = rand \quad (15)$$

A D-dimensional vector, rand, generates a random number between 0 and 1. The object's acceleration (acc) will now be initialized for ith object using equation (16):

$$acc_i = lb_i + rand \times (ub_i - lb_i) \quad (16)$$

Thus, evaluating of the initial population and selecting of the object with best fitness value is carried out. Following, assignment of the den_{best}, Vol_{bert}, and acc_{best}.

Update Densities, Volumes

The density and volume of an object is updated using equation (17):

$$den_i{}^{t+1} = den_i{}^t + rand \times \left(den_{best} - den_i{}^t\right)$$

$$vol_i{}^{t+1} = vol_i{}^t + rand \times \left(vol_{best} - vol_i{}^t\right) \quad (17)$$

Transfer Operator and Density Factor

An object's equilibrium is established when it collides with another object. As stated in (18), AOA's transfer operator TF is used to convert the search from exploration to exploitation.

$$TF = exp\left(\frac{t - t_{max}}{t_{max}}\right) \quad (18)$$

There's a TF out there somewhere. The time will be steadily increased until it reaches one. t and t_{max} are the iterations number and the maximum iterations number. Similarly, AOA benefits from the density-decreasing factor d when conducting global searches down to the neighborhood level. The number of iterations and the maximum iterations number decreases over time, as given by (19).

$$d^{t+1} = exp\left(\frac{t_{max} - t}{t_{max}}\right) - \left(\frac{t}{t_{max}}\right) \quad (19)$$

Exploration Phase

Random material (Mr) and acceleration of object (t + 1) can be used for iteration t+1 if T F≤ 0.5.

$$acc_i{}^{t+1} = \frac{den_{mr} + vol_{mr} \times acc_{mr}}{den^{t+1}{}_i \times vol^{t+1}{}_i} \quad (20)$$

where acc_{mr}, den_{mr} and vol_{mr} indicate a random substance's acceleration, density, and volume. A third of iterations are guaranteed to be spent in exploration if TF is less than 0.5. Exploration and exploitation take on a different dynamic when a value other than 0.5 is employed.

Exploitation Phase

If TF > 0.5 and no objects collide, then use (21) to adjust the object's acceleration for iteration t + 1:

$$acc_i{}^{t+1} = \frac{den_{best} + vol_{best} \times acc_{best}}{den^{t+1}{}_i \times vol^{t+1}{}_i} \quad (21)$$

Where acc_{best} is the best object's acceleration.

Normalize Acceleration

The acceleration can be normalized to determine the change in % by using(22):

$$acc_{i-norm}{}^{t+1} = u \times \frac{acc_i{}^{t+1} - min(acc)}{max(acc) - min(acc)} + l \quad (22)$$

The two normalization ranges u and l is set to 0.90 and 0.1 respectively.

Update Position

If T F ≤ 0.5 (exploration phase), the position of the ith object for the next iteration t + 1 can be expressed as:

$$x_i{}^{t+1} = x^t{}_i + C_1 \times rand \times acc_{i-norm}{}^{t+1} \times d \times (x_{rand} - x_i{}^t) \quad (23)$$

where C1 = 2. Otherwise, if TF > 0.5 (exploitation phase), the objects use this method to update their positions by using equation (24).

$$x_i{}^{t+1} = x^t{}_{best} + F \times C_2 \times rand \times acc_{i-norm}{}^{t+1} \times d \times (T \times x_{best} - x_i{}^t) \quad (24)$$

Where C2 is a constant with a value of 6. T is defined as T =C 3×TF, where T is directly proportional to the transfer operator. T grows over time with range [C3× 0.3, 1]. As a result, the random walk's step size is quite significant because the best and present positions are so vastly different. It steadily increases as the search goes, narrowing the distance between first and second place. Thus, healthy equilibrium between exploration and exploitation can be achieved. Using the flag F, the direction of movement can be changed using (25).

$$F = \begin{cases} +1 \; if \; P \leq 0.5 \\ -1 \; if \; P > 0.5 \end{cases} \quad (25)$$

Where $P = 2 \times rand - C_4$

Evaluation

Evaluating each of the objects can be carried out by using the objective function f with taking into account the best solution found so far. Thus assignment of the den_{best}, Vol_{bert}, and acc_{best} is achieved.

EXTREMUM SEEKING CONTROL SYSTEM

Figure. 4 depicts the classical extremum seeking control (ESC) system as a block diagram.

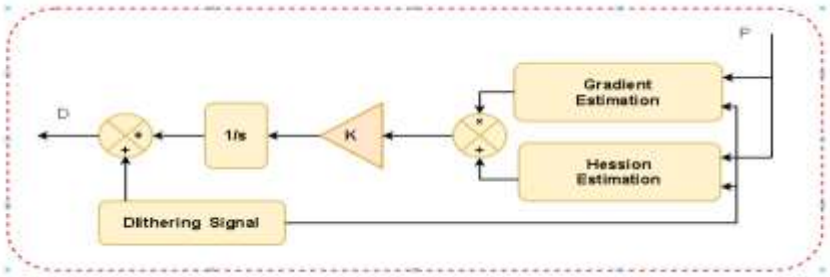

FIGURE 4. Classical ESC scheme

The duty cycle of the PWM signal is controlled by the ESC system. The duty cycle of the ESC is adjusted and sent to the converter in order to get the greatest power point [23].

Classical ESC Model for MPPT

Nonlinear systems can benefit from using ESC to forecast their optimal operating point. Accordingly, this approach may be used to track MPP in solar cells if the system's characteristics curve is concave [23].
As shown in Figure 5, classic ESC is in need of gradient estimator. Considering a nonlinear characteristic curve for solar panel in equation (26):

$$P = \emptyset(X) \tag{26}$$

Where P is the output power of a panel and x is the input that is a function of the signal u. The dithering signal is $u_o \sin(w_o t)$ which results as:

$$P = \emptyset(u + u_o \sin(w_o t) \tag{27}$$

Equation (27) could be approximated by Taylor's series around u as follows:

$$P \approx \emptyset(u) + \frac{d\emptyset(u)}{du} u_o \sin(w_o t) + \frac{1}{4}\frac{d^2\emptyset(u)}{du^2} u_o^2 - \frac{1}{4}\frac{d^2\emptyset(u)}{du^2} u_o^2 \cos(2w_o t) \tag{28}$$

An element with a low frequency and harmonics at frequency make up the panel's output power. When the high-pass filter is applied, the result looks like this.

$$P_f \approx \frac{d\emptyset(u)}{du} u_o \sin(w_o t) - \frac{1}{4}\frac{d^2\emptyset(u)}{du^2} u_o^2 \cos(2w_o t) \tag{29}$$

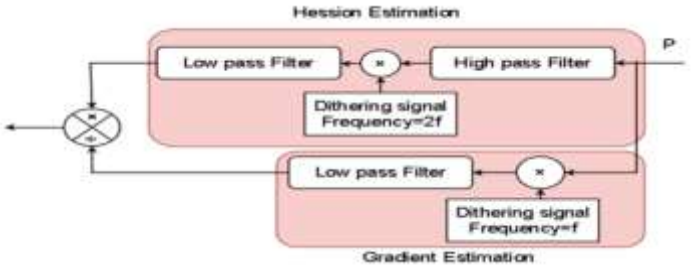

FIGURE 5. Classical ESC estimator

The result of product of the filter output and $u_o^2 cos^2(w_o t)$ is:

$$P_p \approx \frac{1}{2}\frac{d\emptyset(u)}{du} u_o^3 \sin(w_o t) + \frac{1}{4}\frac{d\,\emptyset(u)}{du} u_o^3 \sin(3w_o t) - \frac{1}{4}\frac{d\,\emptyset(u)}{du} u_o^3 \sin(3w_o t) - \frac{1}{8}\frac{d^2\emptyset(u)}{du^2} u_o^2 \cos(2w_o t) - \frac{1}{16}\frac{d^2\emptyset(u)}{du^2} u_o^4 - \frac{1}{16}\frac{d^2\emptyset(u)}{du^2} u_o^4 \cos(4w_o t) \tag{30}$$

When the power signal P_p is pass through a low-pass filter, the output of the ESC system is given as follows:

$$P_{est} \approx -\frac{1}{16}\frac{d^2\emptyset(u)}{du^2} u_o^4 \tag{31}$$

Modified ESC for MPPT

Because a high-pass filter (HPF) and a low-pass filter (LPF) are connected in series to create a band-pass filter (BPF) (LPF). Despite the fact that both the corresponding adapted ESC and the original ESC have the same basic design, the LPF cut-off frequencies in these systems are different... Even though they have similar architecture, both systems are different. As a result, their equations are similar but their performances are different.
If the signal of equation (28) is passing through a HPF the result will be as in equation (32):

$$y_{hpf} \approx f(u) + \frac{1}{4}\frac{d^2 f(u)}{du^2} u_o^2 \tag{32}$$

f(u) variations are slower than their derivative variations because the purpose of a control system design is to improve system performance at the operating point. Therefore as a result of passing the y_{hpf} through a LPF we get:

$$y_m \approx \frac{1}{4}\frac{d^2 f(u)}{du^2} u_o^2 \tag{33}$$

Therefore, to ensure that the DC/DC converter responds quickly to any change in the operating point of PV, the value of u_0 is set to be less than unity.

PROPOSED MPPT SYSTEM

Slower reaction under partial shade conditions, more giant ripple at lower levels of irradiation, and higher oscillation owing to swing around the MPP [24] are some of the downsides of conventional MPPT. In addition, one of most issues of traditional MPPT depends on fixed step-change duty cycle ΔD which is caused in slower response due to assuming constant value. The next duty cycle can be increased or decreased by this value as depicted in equation (34). The proposed hybrid MPPT strategy suggests a duty cycle with each variation in temperature, irradiation and load to solve these issues. In this paper, the suggested MPPT depends on the principle of incremental conductance algorithm, which is $\frac{\mathrm{i_{pv}}}{\mathrm{v_{pv}}} + \frac{\mathrm{di_{pv}}}{\mathrm{dv_{pv}}} = 0$ to investigate the MPP. From this concept, the first step of the proposed MPPT is the calculation of condition by measuring the voltage and current of the PV system and comparing them with zero. The condition of investigating the maximum power point is demonstrated in Figure 6. An incremental conductance controller uses the output error as an input to rectify the system and maximize the amount of electricity harvested from the PV system. For fast tracking of maximum power under non-uniform conditions, the hybrid AOA, algorithm is used to tune the ESC controller. Integral Time Absolute Error (ITAE) is the fitness used to fine-tune the ESC controller's parameters. Equation (35) expresses the ITAE equation

$$D_{i+1} = D_i \mp \Delta D \tag{34}$$

$$j_{min} = \int_0^t t \times \left(\left| 0 - \frac{\mathrm{i_{PV}}}{\mathrm{v_{PV}}} + \frac{\mathrm{di_{PV}}}{\mathrm{dv_{PV}}} \right| \right) dt \tag{35}$$

Where, j_{min} is the minimum fitness and t is simulation error.

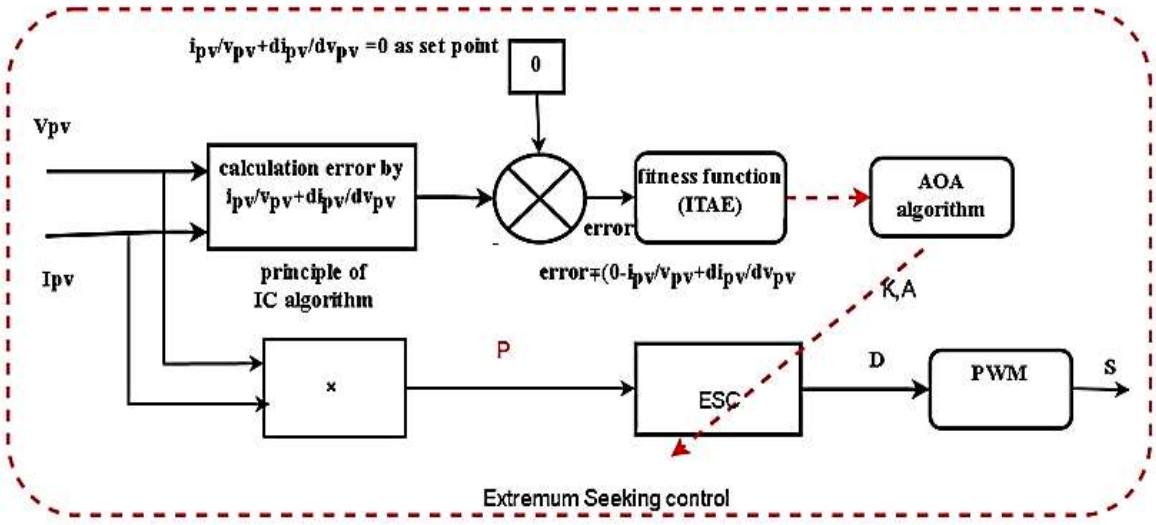

FIGURE 6. A hybrid AOA-ESC proposed MPPT system

SIMULATION RESULTS

Definitions must be clear and precise in order for the parameters to be taken into account and the measurements to be correctly explained. Consequently, new definitions are introduced in a new standard to characterize the total inverter function [25]. MATLAB/Simulink is used to simulate the suggested system. To validate the model and improve the simulation results, the system is evaluated in the context of climate change. Pr EN 50530 [26] test procedures and conditions are used in the testing process.

Irradiation Variation

Figure 7 shows the profile used in this test instance. As shown, the variation occurs between the lowest possible level of radiation, such as 500, and the most significant level conceivable, such as 1000. Furthermore, the temperature is maintained at standard test conditions STC (25 ^{o}C) throughout the irradiation change.

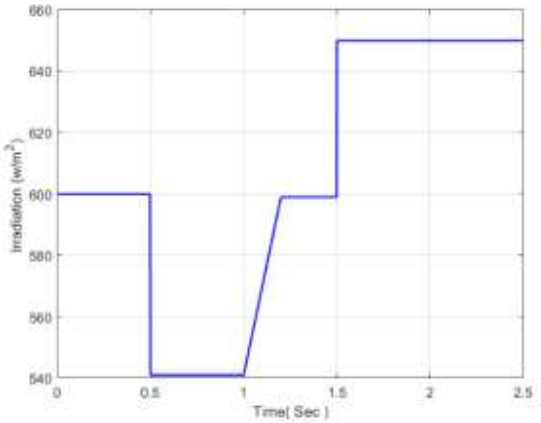

FIGURE 7..Non-uniform irradiance.

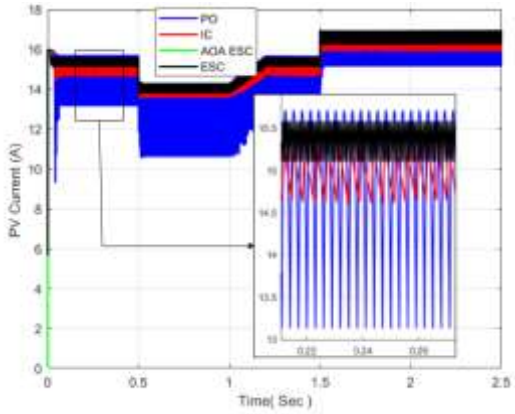

FIGURE 8. PV current response under non-uniform irradiance.

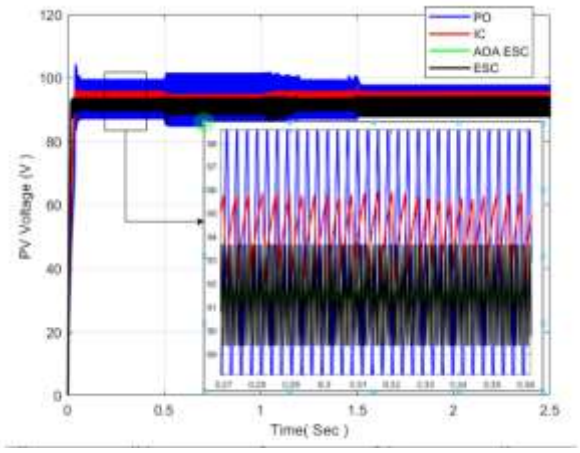

FIGURE.9. PV voltage response under non-uniform irradiance.

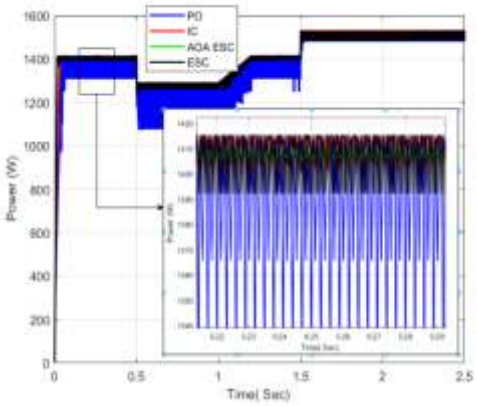

FIGURE 10. PV power of proposed system under non-uniform irradiance.

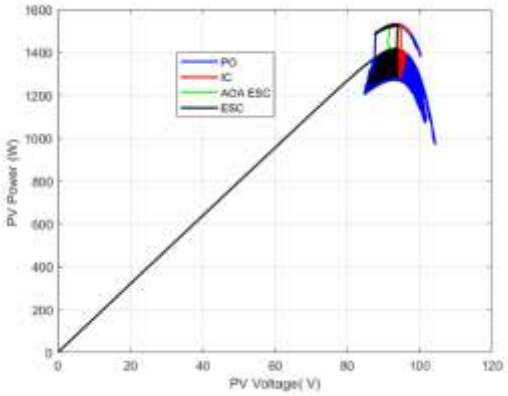

FIGURE 11. PV curve under irradiation variation.

Temperature Variation

Figure. 12 depicts the profile that was employed in this particular test instance. Constant irradiation and temperature variations

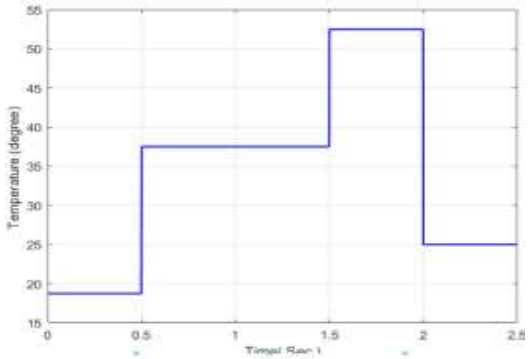

FIGURE 12. Profile of temperature. change

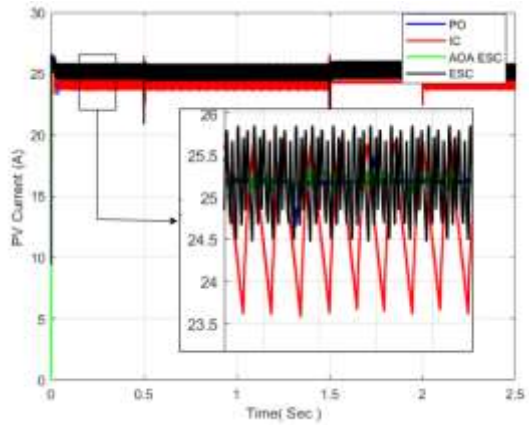

FIGURE 13.. Dynamic response of PV current under variable temperature

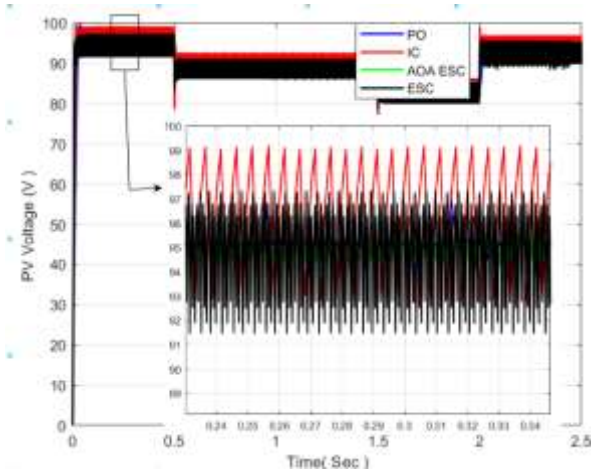

FIGURE 14.. Dynamic response of PV voltage under variable temperature

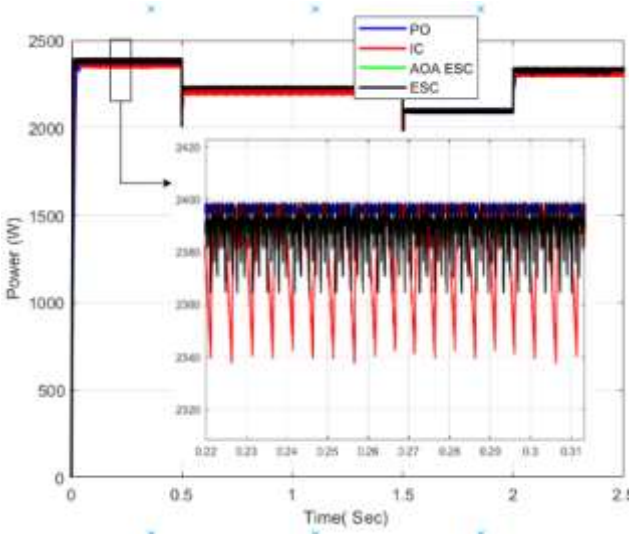

FIGURE 15. Dynamic response of PV power under variable temperature

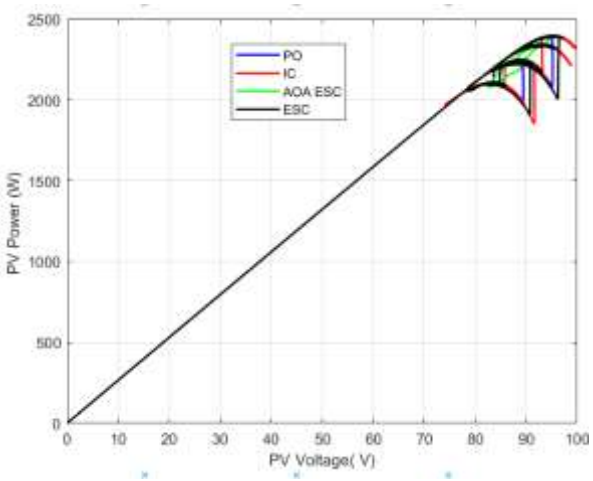

FIGURE 16. P-V curve under temperature variation

Simultaneous Variations of Irradiation and Temperature

Finally, the system is tested with combination of irradiance and temperature changes. Figures 17 and 18 depict the profiles of this test. As shown, there are abrupt and gradual variations in irradiance and temperature. For the PV system, these variation represent a random and unpredictable operating condition.

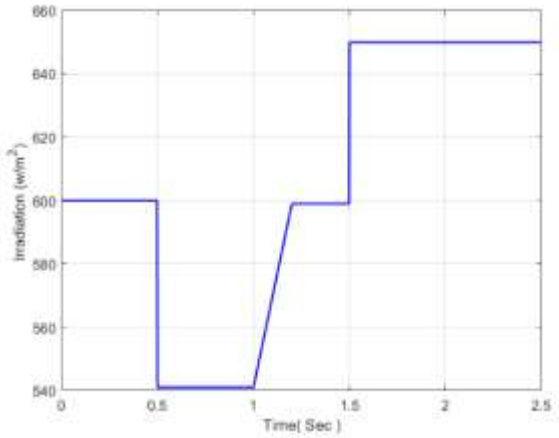

..

FIGURE 17. Profile of irradiance variation

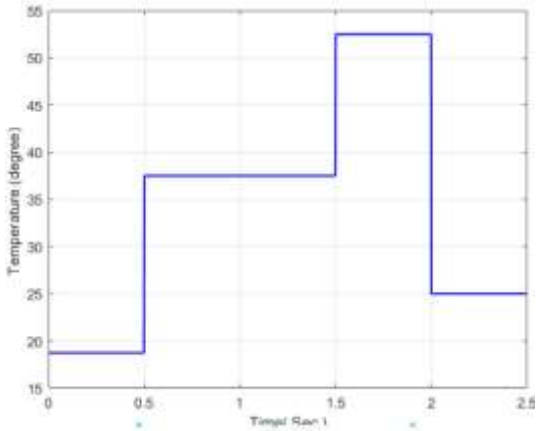

FIGURE 18. Profile of variable temperature.

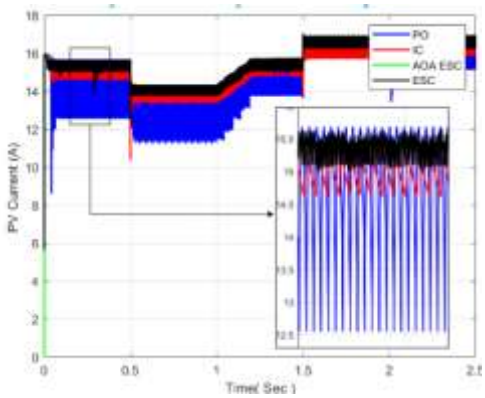

FIGURE 19. Dynamic response of PV current under variable irradiance and temperature

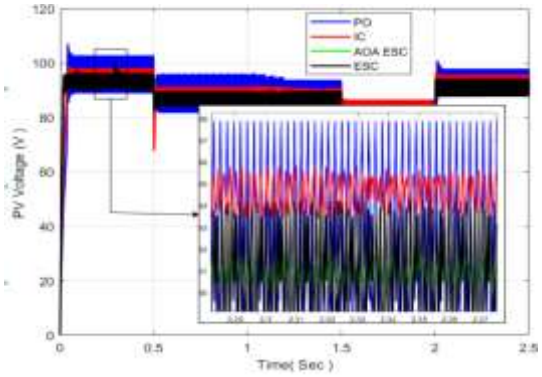

FIGURE 20. Dynamic response of PV voltage under variable irradiance and temperature

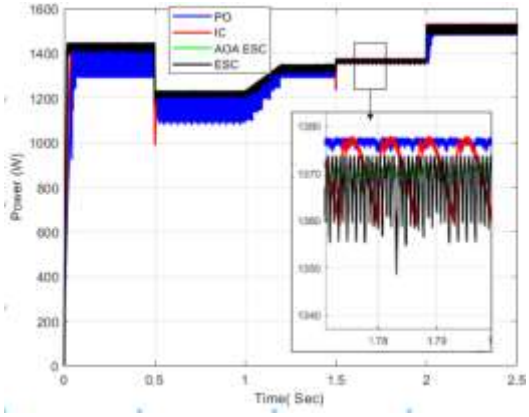

FIGURE 21. Dynamic response of PV power under variable irradiance and temperature

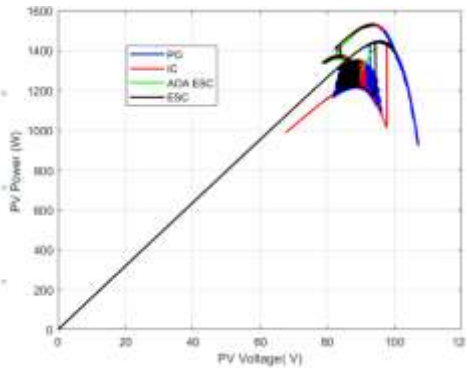

FIGURE 22. P-V curve under variation irradiation and temperature.

Comparisons Performance Among the MPPT Strategies

As demonstrated by the previous findings, the suggested AOA-based ESC algorithm has a faster tracking speed and better efficiency and power quality compared with the conventional ones.

Tables 1 and 2 show the indices used to determine the power response under varying conditions for the proposed MPPT algorithms and standard methods. The proposed AOA-based ESC MPPT algorithm outperforms the ESC MPPT and conventional PO and IC algorithms in all system responses. The AOA-based ESC MPPT beat the PO and IC algorithms in this regard, as seen in the tables.

TABLE 1. Performances comparisons of proposed MPPT with Conventional MPPT algorithms under variation irradiation.

Performance Index	P&O MPPT	IC MPPT	ESC MPPT	AOA- ESC MPPT
Accuracy, α_{MPPT}	94.34	95.61	97.842	99.450
Static efficiency, η_{MPPT}	94.012	95.301	97.7445	99.650
Relative tracking error, ϵ_{MPPT}	5.42	4.73	2.955	1.113
Energetic efficiency, $\eta_{MPPT.\ E}$	94.501	95.63	97.685	99.558
Energetic error, $\epsilon_{MPPT.\ E}$	5.57	4.89	3.115	1.2502

TABLE 2. Specification performances under variation irradiation.

Index	P&O MPPT	IC MPPT	ESC MPPT	AOA-ESC MPPT
Rise time (ms)	10.124	9.714	4.90	3.312
Settling time(ms)	13. 5	10.042	7.40	4.82
Overshoot (watt)	47.5	23.145	8.1345	0.3302
undershoot(watt)	85.47	38.145	9.41	0.402
Ripple(watt)	400.2	150.42	20	1.40

CONCLUSION

This study demonstrates a modified MPPT algorithm based on a novel ESC and the idea of incremental conductance (IC) algorithm. AOA is the proposed optimizer for fine-tuning these two parameters. An MPPT that can be easily implemented, be more efficient, and address various challenges is a significant advantage for the proposed method. High-speed MPP tracking, no overshoot or oscillation, and a 99.65% efficiency level are some of the advantages of the proposed algorithm compared to standard MPPT and numerous clever algorithms. Using AOA-based ESC MPPT, there is no failure rate, a convergence time of less than 0.031 s, and zero oscillations around steady-state conditions for any partial shadow situations,

REFERENCES

1. A. Azman, A. Rahman, N. Bakar, F. Hanaffi and A. Khamis, presented at the 2011 IEEE Conference on Clean Energy and Technology (CET), 2011 (unpublished).
2. S. Tan, W. Ho, H. Hashim and C. Lee, presented at the 2014 International Conference and Utility Exhibition on Green Energy for Sustainable Development (ICUE), Thailand, 2014 (unpublished).
3. B. K. Bose, IEEE Industrial Electronics Magazine 4 (1), 6-17 (2010).
4. S. R. Bull, Proceedings of the IEEE 89 (8), 1216-1226 (2001).
5. D. C. Huynh and M. W. Dunnigan, IEEE Transactions on Sustainable Energy 7 (4), 1421-1429 (2016).
6. T. Radjai, L. Rahmani, S. Mekhilef and J. P. Gaubert, Solar Energy 110, 325-337 (2014).
7. A. S. Blazev, *Photovoltaics for commercial and utilities power generation*, 1st ed. (River Publishers, NC, USA, 2020).
8. N. Karami, N. Moubayed and R. Outbib, Renewable and Sustainable Energy Reviews 68, 1-18 (2017).
9. M. Seyedmahmoudian, B. Horan, T. K. Soon, R. Rahmani, A. M. T. Oo, S. Mekhilef and A. Stojcevski, Renewable and Sustainable Energy Reviews 64, 435-455 (2016).
10. R. Faranda and S. Leva, WSEAS transactions on power systems 3 (6), 446-455 (2008).
11. Y. H. Liu, S. C. Huang, J. W. Huang and W. C. Liang, IEEE Transactions on Energy Conversion 27 (4), 1027-1035 (2012).
12. Y. Wang, Y. Li and X. Ruan, IEEE Transactions on Industrial Electronics 63 (1), 235-245 (2016).

13. Y. Ji, D. Jung, J. Kim, J. Kim, T. Lee and C. Won, IEEE Transactions on Power Electronics 26 (4), 1001-1009 (2011).
14. K. Harada and G. Zhao, IEEE Transactions on Power Electronics 8 (4), 654-662 (1993).
15. E. Bianconi, J. Calvente, R. Giral, E. Mamarelis, G. Petrone, C. A. Ramos-Paja, G. Spagnuolo and M. Vitelli, International Journal of Electrical Power & Energy Systems 44 (1), 346-356 (2013).
16. L. Jin-Gook, K. Jae-Sub, J. Da-Eun, J. Hak-Gyun, K. Dae-Kyong and C. Dong-Hwa, presented at the 2012 IEEE Vehicle Power and Propulsion Conference, 2012 (unpublished).
17. P. Lei, Y. Li and J. E. Seem, IEEE Transactions on Sustainable Energy 2 (3), 348-358 (2011).
18. M. A. E. H. Mohamed, presented at the 2015 IEEE 42nd Photovoltaic Specialist Conference (PVSC), 2015 (unpublished).
19. R. Cuzco, D. Arcos-Aviles and J. Llanos, presented at the Proc. XVI Multidisciplinary International Congress on Science and Technology, 2021 (unpublished).
20. S. Muthukaruppasamy, A. Abudhahir, A. G. Saravanan, J. Gnanavadivel and P. Duraipandy, Journal of Electrical Engineering and Technology 13 (5), 1886-1900 (2018).
21. H. A.-K. Hussein and H. J. Motlak, Indonesian Journal of Electrical Engineering and Computer Science 25 (2), 710-720 (2022).
22. F. A. Hashim, K. Hussain, E. H. Houssein, M. S. Mabrouk and W. Al-Atabany, Applied Intelligence 51 (3), 1531-1551 (2021).
23. H. Heydari-doostabad, R. Keypour, M. R. Khalghani and M. H. Khooban, Solar Energy 94, 28-36 (2013).
24. M. Sarvi and A. Azadian, Energy Systems, 1-40 (2021).
25. Final draft FprEN 50530, Overall efficiency of PV inverters, CENELEC (December 2008).
26. R. Bründlinger, N. Henze, H. Häberlin, B. Burger, A. Bergmann and F. Baumgartner, presented at the 24th EU PV Conf., Hamburg, Germany, 2009 (unpublished).